3D Graphene/silk fibroin scaffolds enhance dental pulp stem cell osteo/odontogenic differentiation

Sergio López-García [a,1], Salvador D. Aznar-Cervantes [b,1], Ana Pagán [b], Carmen Llena [a], Leopoldo Forner [a], José L. Sanz [a], David García-Bernal [c], Sonia Sánchez-Bautista [d], Laura Ceballos [e], Victoria Fuentes [e], María Melo [a], Francisco J. Rodríguez-Lozano [f,*], Ricardo E. Oñate-Sánchez [f]

[a] Departament d'Estomatologia, Facultat de Medicina I Odontologia, Universitat de València, Valencia 46010, Spain
[b] Biotechnology, Genomics and PlantBreedingDepartment, Instituto Murciano de Investigación y Desarrollo Agrario y Ambiental (IMIDA), La Alberca 30150, Murcia, Spain
[c] Department of Biochemistry, Molecular Biology B and Immunology, Faculty of Medicine, University of Murcia, Biomedical Research Institute (IMIB), Murcia 30120, Spain
[d] Faculty of Medicine, Catholic University San Antonio of Murcia, Murcia 30107, Spain
[e] IDIBO Research Group, Area of Stomatology, Health Sciences Faculty, Rey Juan Carlos University, Alcorcón, Madrid, Spain
[f] Department of Dermatology, Stomatology, Radiology and Physical Medicine, Morales Meseguer Hospital, Biomedical Research Institute (IMIB), Regional Campus of International Excellence "Campus Mare Nostrum", Faculty of Medicine, University of Murcia, Murcia 30008, Spain

ARTICLE INFO

ABSTRACT

Objectives: The current in vitro study aims to evaluate silk fibroin with and without the addition of graphene as a potential scaffold material for regenerative endodontics.

Material and Methods: Silk fibroin (SF), Silk fibroin/graphene oxide (SF/GO) and silk fibroin coated with reduced graphene oxide (SF/rGO) scaffolds were prepared (n = 30). The microarchitectures and mechanical properties of scaffolds were evaluated using field emission scanning electron microscopy (FESEM), pore size and water uptake, attenuated total reflectance fourier transformed infrared spectroscopy (ATR-FTIR), Raman spectroscopy and mechanical compression tests. Next, the study analyzed the influence of these scaffolds on human dental pulp stem cell (hDPSC) viability, apoptosis or necrosis, cell adhesion, odontogenic differentiation marker expression and mineralized matrix deposition. The data were analyzed with ANOVA complemented with the Tukey post-hoc test ($p < 0.005$).

Results: SEM analysis revealed abundant pores with a size greater than 50 nm on the surface of tested scaffolds, primarily between 50 nm and 600 μm. The average value of water uptake obtained in pure fibroin scaffolds was statistically higher than that of those containing GO or rGO ($p < 0.05$). ATR-FTIR evidenced that the secondary structures did not present differences between pure fibroin and fibroin coated with graphene oxide, with a similar infrared spectrum in all tested scaffolds. Raman spectroscopy showed a greater number of defects in the links in SF/rGO scaffolds due to the reduction of graphene. In addition, adequate mechanical properties were exhibited by the tested scaffolds. Regarding biological properties, hDPSCs attached to scaffolds were capable of proliferating at a rate similar to the control, without affecting their viability over time. A significant upregulation of *ALP*, *ON* and *DSPP* markers was observed with SF/rGO and SF/GO groups. Finally, SF/GO and SF/rGO promoted a significantly higher mineralization than the control at 21 days.

Significance: Data obtained suggested that SF/GO and SF/rGO scaffolds promote hDPSC differentiation at a genetic level, increasing the expression of key osteo/odontogenic markers, and supports the mineralization of the extracellular matrix. However, results from this study are to be interpreted with caution, requiring further in vivo studies to confirm the potential of these scaffolds.

* Corresponding author.
  E-mail address: fcojavier@um.es (F.J. Rodríguez-Lozano).
[1] These authors contributed equally to this work.

S. López-García et al.

1. Introduction

In recent decades, with the emergence of regenerative dentistry, new therapeutic approaches have shifted towards a biological perspective, by applying materials with a biological activity (i.e., by enhancing the osteo-dentinogenic cellular activity) [1,2]. In this regard, the application of reparative/regenerative techniques are sought with the aim of resolving destructive processes, such as root perforations or resorptions; and to maintain the tooth's vitality by the repair/regeneration of non-mineralized dental tissues [3,4]. Autologous grafts have been described as the gold standard therapy; however, their use is limited due to by low harvesting and availability and donor site pain [5]. Therefore, new strategies have been proposed to use new materials or composites in regenerative endodontics [6].

Silk fibroin (SF) is a natural polymeric product with a long tradition as a biomaterial, but with a limited application.The advantages of SF over other biomaterials lie in its low cost, excellent mechanical properties, high biocompatibility, water-based processing, biodegradability, and the presentation of easily accessible chemical groups to introduce functional chemical modifications [7–11]. However, their odonto/osteoblastic potential is very discrete, which limits its application [12].

On the other hand, graphene is commonly grouped as a family of carbonaceous nanomaterials with different oxidation states, and several configurations have been described for tissue engineering applications [13]. Specific formulations of graphene have demonstrated a high biocompatibility and implantation potential, expanding the possibilities for its biomedical applications, such as gene or drug delivery. In addition, several published works report the adequate cellular biocompatibility or cytocompatibility of graphene surfaces [14]. Graphene oxide (GO) is a 2D carbon allotrope with a single layer hexagonal structure, avery high surface to volume ratio and amazing mechanical properties [15–17]. This material has shown desirable and singular properties in the field of physics, including increased electrical and thermal conductivity, high mechanical resistance and excellent optical properties. GO modification is commonly used to improve the biomechanical properties of scaffolds and to promote cell adhesion, proliferation, and differentiation. In fact, it has been shown to be a favorable scaffold material for tissue-engineered bone, and bidimensional (2D) SF scaffolds supplemented with GO supported cell growth and osteo/cementogenic differentiation of human mesenchymal stromal from different sources such as bone marrow and periodontal ligament [12,18–20]. Reduced graphene oxide (rGO), a new form resulting from the reduction of GO by either chemical or microwave methods, has shown to be both biocompatible and to have osteoinductive activity in vitro. However, this form has not been evaluated with dental pulp cells and using a 3D scaffold. Therefore, in this study, as a preliminary step to investigate its beneficial properties in vivo using a model of dental pulp repair, we hypothesized that SF coated with GO or rGO, in a 3D conformation, would promote a significantly higher differentiation than SF.

2. Materials and methods

2.1. Silk processing and fabrication of 3D porous scaffolds

Bombyx mori cocoons were obtained from silkworms reared in the sericulture facilities of the IMIDA (Murcia, Spain) and graphene oxide (GO) water dispersion (4 mg/mL) was provided by GRAPHENEA (San Sebastian, Spain). To develop the silk fibroin (SF) materials, silkworm cocoons were segmented into four or five pieces and boiled in 0.02 M Na_2CO_3 for 30 min to remove the glue-like sericin proteins. Raw SF was then thoroughly rinsed with water and dried at room temperature for three days. The extracted SF was then dissolved in 9.3 M LiBr (Acros Organics, Geel, Belgium) for three hours at 60 ºC to generate a 20% w/v solution, which was dialyzed against distilled water for three days (Snakeskin Dialysis Tubing 3.5 kDa MWCO, Thermo Fisher Scientific, Waltham, MA, United States), with a total of eight water changes. The

resulting 7–8% w/v SF solution was collected, filtered, and stored at 4 ºC for no longer than 30 days. This solution was used for scaffold fabrication.

To prepare the fibroin scaffolds, 8.8 cm diameter petri dishes were used as moulds. Fifteen grams of NaCl (grain size 400–600 μm) was used as a porogen and uniformly deposited on them. Next, 8 mL of SF solution (7.5% w/v) was poured onto the NaCl bed, and the protein was allowed to coagulate for 48–72 h. Afterwards, a compact paste was produced and treated with methanol for an hour to increase the beta-sheet content of fibroin, thereby contributing to the effective insolubilization of this protein and giving the scaffolda greater structural integrity. The 6.9 mm diameter discs were then punched out of the petri dish. They were washed for 48 h with successive changes of milliQ water (at least six water changes). This ensured the removal of NaCl, leaving in its place an interconnected porous network with a sponge-like appearance [21]. A portion of the SF materials were coated with GO by means of immersion in aqueous suspensions of GO at 4 mg·mL^{-1}. Five cycles of immersion in these aqueous suspensions of GO were performed, alternating with periods of drying (at 45 ºC for 30 min). Some of the materials were then immersed in an aqueous solution of ascorbic acid (20 mM) for three hours at 70 ºC, following the method proposed by Fernández-Merino et al. for the reduction of GO and previously used by our research group with other types of fibroin biomaterials [19,22]. Therefore, three types of scaffolds were studied; on one hand, pure fibroin materials without incorporated GO were used as negative controls and designated as "SF". On the other hand, the SF scaffolds containing GO adsorbed on their surface were termed as "SF/GO", and those in which the superficially adsorbed GO was reduced were termed "SF/rGO".

2.2. Pore size measurement and water uptake analysis

SEM was used to acquire micrographs of the unseeded scaffolds to correctly visualize their topography and measure the size of their pores, based on their maximum width (three scaffolds per treatment) using image J software. 30 pores (10 per replica) were measured at two magnifications (50x and 3000x). The statistical analyses of the two were performed separately, since they represent two different approaches. The methodology and equipment used for this technique is the same as described later, in Section 2.8 related to cell adhesion.

Parallly, to calculate water uptake (%), the wet (Ww) and dry (Wd) weights of four scaffolds per treatment were recorded. The values were calculated using the following formula [6]:

$$Water \quad uptake = \left(\frac{Ww - Wd}{Ww} \right) * 100$$

2.3. Evaluation of mechanical properties

Mechanical compression tests were performed on the scaffolds (either in dry or in wet state) using a universal testing frame machine (Qtest; MTS Systems, Eden Prairie, MN, United States). The mechanical properties of the specimens were recorded using a 200 N load cell at a rate of 5 mm/min until a 60% strain level was reached. Three specimens per treatment were analysed. Each specimen was approximately 6–7 mm in diameter and 2 mm in height.The exact dimensions of the scaffolds were determined immediately prior to testing. The compression modulus (kPa) was calculated from the slope of the stress-strain curves between 5% and 10% of deformation (elastic linear portion), while the values of compressive force (N) and compressive strength (kPa) were recorded at 60% of deformation, in a similar way to that previously proposed by several authors [23,24]. An initial compressive contact to 0.05 N was applied to ensure complete contact between the specimen and the surface. For the wet tests, the dried scaffolds were pre-hydrated forone hour in 1X PBS.

2.4. Attenuated total reflectance fourier transformed infrared spectroscopy (ATR-FTIR)

ATR-FTIR was used to analyse the structural changes or the possible influence of the presence of GO on the molecular conformation of the electrospun SF mats. Each spectrum was acquired on a Nicolet iS5 spectrometer, equipped with an iD5 ATR accessory (Thermo Fisher Scientific) and controlled with the OMNIC™software (ver. 9.3.30). Measurements were performed in absorbance mode with a resolution of 4 cm^{-1}, a spectral range of 4000–550 cm^{-1}, and 64 scans. The relative percentages of the secondary structures were calculated from the areas of the corresponding Gaussian functions as previously published by our research group [25].

2.5. Raman spectroscopy

Raman spectroscopy was used to study the structural characteristics of the SF and SF/GO scaffolds. Spectra from different regions of the dust samples were recorded in a Renishaw spectrometer (In Via, United Kingdom) with an excitation wavelength of 514 nm generated by an AR+ laser. The spectral range of 100–3500 cm^{-1} was evaluated using 10 scans for each measurement. The samples were focused using a Leica optical microscope (Leica, Wetzlar, Germany) at 50x magnification. Prior to the analysis, the value of the Raman shift was calibrated against the line at 520 cm^{-1} using a sample of pure silicon.

2.6. Cell culture

The protocol to obtain human dental pulp stem cell (hDPSCs) was approved by the ethical committee of the University of Murcia (Murcia, Spain; IRB number 3686/2021). Informed consent was obtained from ten patients (18–23 years old), who provided molars from which hDPSCs were isolated and agreed to their use in this study. Dental pulp tissues were aseptically removed and immersed for incubation in 0.25% trypsin in four mL of EDTA (Life Technologies, Carlsbad, CA, United States) for 30 min at 37 °C. After neutralization with four mL of medium, the cells were detached by forced pipetting and then they were filtered through a 70 μm cell strainer (Corning, Corning, NY, United States). The hDPSCs were cultured in Dulbecco's modified Eagle's medium containing 10% fetal bovine serum, penicillin (100 U/mL), streptomycin (100 μg/mL) and 1% L-glutamine (all from Gibco, Life Technologies, Carlsbad, CA, United States) supplemented with 100 mM ascorbic acid (Sigma Aldrich, St. Louis, MO, United States) (complete growth medium) in a 37 °C incubator with 5% CO_2 (Thermo Forma 3110, Thermo Fisher Scientific). hDPSCs of passages three to five were used in this study and were characterized as mesenchymal stem cells based on a previous similar study [26].

2.7. Cytocompatibility and apoptosis/necrosis assay

The assay was performed in 96-well plates containing the tested materials (SF, SF/GO and SF/rGO), and a control without scaffolds. 1×10^3 cells were seeded per well in 180 μL of DMEM culture medium with phenol red (Gibco) supplemented with 1% L-glutamine, 10% SBF and penicillin/streptomycin (100 μg/mL) and were incubated at 37ºC and 5% CO_2. After the incubation period, the culture medium was replaced with 200 μL of DMEM without phenol red, and a resazurin-based assay according to the manufacturer's recommended protocol (Alamar blue, ThermoFisher Scientific). Cytocompatibility was analyzed at 24, 48, and 72 h of culture with or without the tested scaffolds (negative control). Resazurin reduction was determined by measuring the relative fluorescence (excitation at 560 nm and emission at 590 nm). Three independent experiments were performed, testing three samples per group.

To assess apoptosis/necrosis, hDPSCs were cultured with the different materials for 21 days, followed by a double staining with

Annexin-V and 7-AAD (BD Biosciences, San Jose, CA, United States). After the incubation period, the hDPSCs were detached from the culture flask and washed as described previously [26]. They were then incubated with phycoerythrin-conjugated Annexin-V and 7-AAD in binding buffer for 15 min at room temperature. The percentage of live cells (Annexin-V−/7-AAD−), early apoptotic (Annexin+/7-AAD−), or late apoptotic and/or necrotic cells (Annexin-V+/7-AAD+ and Annexin-V-/7-AAD+) was analyzed by flow cytometry using a BD FACS Canto flow cytometer (Becton Dickinson, Franklin Lakes, NJ, United States). All determinations were performed in triplicate.

2.8. Cell adhesion

The morphology of hDPSCs adhered to the scaffolds was evaluated after 72 hours by scanning electron microscopy (SEM) (n = 3). Scaffolds were fixed with 2% glutaraldehyde in 0.1 M cacodylate buffer for 30 min at 4ºC. They were then rinsed and post fixed in osmium tetroxide for one hour before being dehydrated through increasing concentrations of ethanol (30, 50, 70, 90 vol%), with a final dehydration in absolute alcohol. They were then dried by the critical point method and coated with gold and palladium. The materials were examined using a Jeol 6100 unit (Jeol, Tokyo, Japan) at 400x, 800x and 1600x magnification.

2.9. Gene expression

To determine the mRNA transcript levels of the odonto/osteogenic differentiation and mineralization markers, the hDPSCs were cultured together with the tested scaffolds. Real-time quantitative polymerase chain reaction (RT-qPCR) was performed to quantify gene expression. Twenty thousand hDPSCs per well were seeded onto 12-well plates (n = 3) and incubated for 7 and 21 days with the scaffolds in unconditioned culture medium (negative control group), or in osteogenic differentiation medium (OsteoDiff®media; MiltenyiBiotec, BergischGladbach, Germany; positive control group). Culture media were changed every three days. The primer sequences for the differentiation markers were as follows (5–3'):alkaline phosphatase (*ALP*): 5′-TCAGAAGCTCAACACCAACG-3′/5′-TTGTACGTCTTGGAGAGGGC-3′; collagen type 1 (*Col1A1*): 5′-CCCGGGTTTCAGAGACAACTTC-3′/5′-TCCACATGCTTTATTCCAGCAATC-3′; osteonectin (*ON*): 5′-GCAT-CAAGCAGAAGGATA-3′/5′-AATAGTTAAGTTACAGCTAAGAAT-3′; dentin sialophosphoprotein (*DSPP*): 5′-GCATTTGGGCAGTAGCATGG-3′/5′-CTGACACATTTGATCTTGCTAGGAG-3′; and runt-related transcription factor 2 (*RUNX2*): 5′-TCCACACCATTAGGGACCATC-3′/5′-TGCTAATGCTTCGTGTTTCCA-3′; bone sialoprotein or BSP: 5′-TGCCTTGAGCCTGCTTCCT-3′/5′-CTGAGCAAAATTAAAG-CAGTCTTCA-3′;amelogenin X or AMELX: 5′-CACCCTGCAGCCTCAT-CACC-3′/5′-GTGTTGGATTGGAGTCATGG-3′;Ameloblastin or AMBN: 5′-AGCCATGTTTCCAGGATTTG-3′/5′-TGCACCTCCTTCTTCGTTCT-3′;Glyceraldehyde 3-phosphate dehydrogenase (GAPDH) was used as housekeeping gene to quantify and normalize the results, with the following primers sequences (forward/reverse): 5′-TCAG-CAATGCCTCCTGCAC-3′/5′-TCTGGGTGGCAGTGATGG-3′. Three independent samples per treatment and time were tested.

2.10. Mineralization assay

The cell seeding procedure and the experimental groups were the same as for the gene expression assay, including negative and positive (OsteoDiff) controls. The culture medium was changed every 3–4 days. After 21 days of culture, the cells were washed twice with PBS and fixed with 10% formalin neutral buffer solution (Wako Pure Chemical Industries Ltd, Osaka, Japan) at room temperature for 10 min, and then washed twice with PBS and twice with DDW. Monolayers were stained with 1 mL/well 40 mM Alizarin Red S (Wako Pure Chemical Industries Ltd) for one hour at the stirring stage. The samples were then washed with DDW twice and PBS once. The samples were photographed using a

ARTICLE IN PRESS

S. López-García et al.   Dental Materials xxx (xxxx) xxx

4×10.13 php, UP Lan FL lens under a light microscope (Olympus CKX41; Olympus, Tokyo, Japan). The dye was then extracted from the plate by incubation in 200 μL/well 10% cetylpyridium chloride (NacalaiTesque Inc., Kyoto, Japan) for 20 min and transferred to a 96-well microplate. Colorimetry was assessed by absorbance at 577 nm using a microplate reader. Three independent samples per treatment and time were tested.

2.11. Statistical analysis

All data presented are from experiments performed three times. For quantification, data were calculated as mean and standard deviation (SD). The normality of the data distribution was first confirmed using a Q-Q plot. Statistical significance was tested by one-way ANOVA followed byTukey's post hoc test using Graph-Pad Prism v8.1.0 (GraphPad Software, La Jolla, CA, United States). Here, * indicates a P-value less than 0.05, * * indicates a P-value less than 0.01, and * ** indicates a P-value less than 0.001.

Only the data related to pore size did not meet the requirement of normality, and therefore the comparison of their mean values was carried out using the non-parametric test of Mann-Whitney ($p < 0.05$).

3. Results

3.1. Pore size and water uptake

To characterize the porous structure of the different scaffolds, they were visualized by FESEM at different magnifications. Pore sizes were measured as described in the Material and Methods section.The mean values are shownin Table 1. No significant differences were detected in the pore sizes observed at 50x between the three scaffolds tested ($p > 0.05$). As shown in the first column of Fig. 1, trabecular-like structures interconnected by an equivalent macroporosity can be observed.

However, statistically significant differences were found when analysing of the smaller pores at 3000x. Pure silk fibroin (SF) scaffolds had a significantly smaller mean pore size ($p < 0.05$) compared to SF/GO and SF/rGO scaffolds, the latter being statistically similar ($p > 0.05$). This result can be explained by the obstruction of the smaller pores of SF by the GO or rGO coverage and is consistent with what is observed in the second column of Fig. 1. The mean water uptake value obtained in pure fibroin scaffolds was statistically higher than in SF/GO or SF/rGO ($p < 0.05$). Again, SF/GO and SF/rGO scaffolds were similar in this regard ($p > 0.05$).

3.2. Mechanical properties

The mechanical behaviour of the materials tested was characterized by means of compression tests carried out on the scaffolds (either in a dry or wet state). The values of compressive modulus (kPa), compressive force (N) and compressive strength (kPa) are presented in Table 2. In the dry state, the SF scaffolds exhibited a significantly higher value than the other scaffolds in all the parameters ($p < 0.05$), showing a greater

rigidity and resistance than those with GO on their surface. On the other hand, no significant differences were observed between the three types of scaffolds in the wet state tests ($p > 0.05$).

3.3. Infrared spectroscopy and microstructural characterization

Infrared spectroscopy was used to investigate the secondary structure content of the tested materials, as previously described. The complete infrared spectra show the presence of amide I (1620 cm^{-1}), amide II (1514 cm^{-1}), amide III (1229 cm^{-1}), and amide IV (1061 cm^{-1}) peaks in all the tested materials(Fig. 2A). For comparison purposes, pure GO and rGO films manufactured by evaporation on glass slides were included in the analysis. In those of GO, an intense band appears between 3000 cm^{-1} and 3500 cm^{-1} (Fig. 2A), which represents O-H stretching vibrations. This was also observed in the SF/GO scaffold, but after the reduction step, this band disappeared, both in the pure rGO film and in the SF/rGO scaffold. Regarding the microstructural characterization, after deconvoluting the amide I peak, as shown in Fig. 2B and Table 3, no significant differences were detected in any of the studied secondary structures ($p > 0.05$).

3.4. Raman spectroscopy

The samples were then analyzed by Raman spectroscopy to obtain evidence for the presence of GO in the scaffolds. The spectrum obtained for SF scaffolds was as expected in a sample of silkworms' fibroin (Fig. 2C). In the case of scaffolds coated with GO, the D band, located close to 1300 cm^{-1}, represents the presence of defects in the hexagonal structure of the GO while the G band (graphitic, located around 1500 cm^{-1}) is associated with the sp2 carbon structures. In the case of the SF/GO, the peak at close to 1300 cm^{-1} presents a lower intensity than that of 1500 cm^{-1} with a ratio of 0.924. However, in SF/rGO, the intensity is greater than 1300 cm^{-1} and the ratio is 1.187, indicating a greater number of bonding defects due to GO reduction.

3.5. Cytocompatibility and apoptosis/necrosis assay

Cytocompatibility of the different materials was assessed using a resazurin-based assay. An increase in cell proliferation is associated with increased signalling, whereas a decrease in cell proliferation indicates a lower cytocompatibility of the compounds tested. As shown in Fig. 2D, there were no significant differences between the SF/GO and the control groups at 24 h of culture, nor between the SF and SF/rGO groups and the scaffold-free cells (control)after 48 h. After 48 and 72 h of culture, cell proliferation was significantly increased in the SF/GO group compared with the control group ($p < 0.001$). Cell proliferation was significantly decreased in the SF group at 24 h and 72 h compared to the control groups. In general, the three types of scaffolds showed adequate cell proliferation. On the other hand, the apoptosis/necrosis assay revealed > 98% cell viability in all groups, confirming the cytotocompatibility of the tested scaffolds (Supplementary Fig. 1).

3.6. Cell adhesion

SEM was used to determine hDPSC morphology on the surface of the scaffolds after 72 hours of culture. Abundant and well-adherent cells were observed on the surface of the three types of scaffolds (SF, SF/GO and SF/rGO). The cells showed the typical fibroblastic morphology of hDPSCs with numerous cytoplasmic extensions (Fig. 3 and Supplementary Fig. 2).

3.7. Gene expression

The osteogenic and odontogenic potential of the tested scaffolds on hDPSCs was investigated by analysing of the expression of the osteogenic and odontogenic related genes *ALP, Col1A1, RUNX2, ON, BSP,*

Table 1
Mean values of pore size (observed at 50x and 300x) and water uptake of the different silk fibroin (SF) scaffolds produced. "GO" or "rGO" refers to the presence of graphene oxide or reduced graphene oxide in the composition of the scaffolds, respectively. The data are expressed as mean values ± standard error of the mean.* Indicates significantly different values ($p < 0.05$).

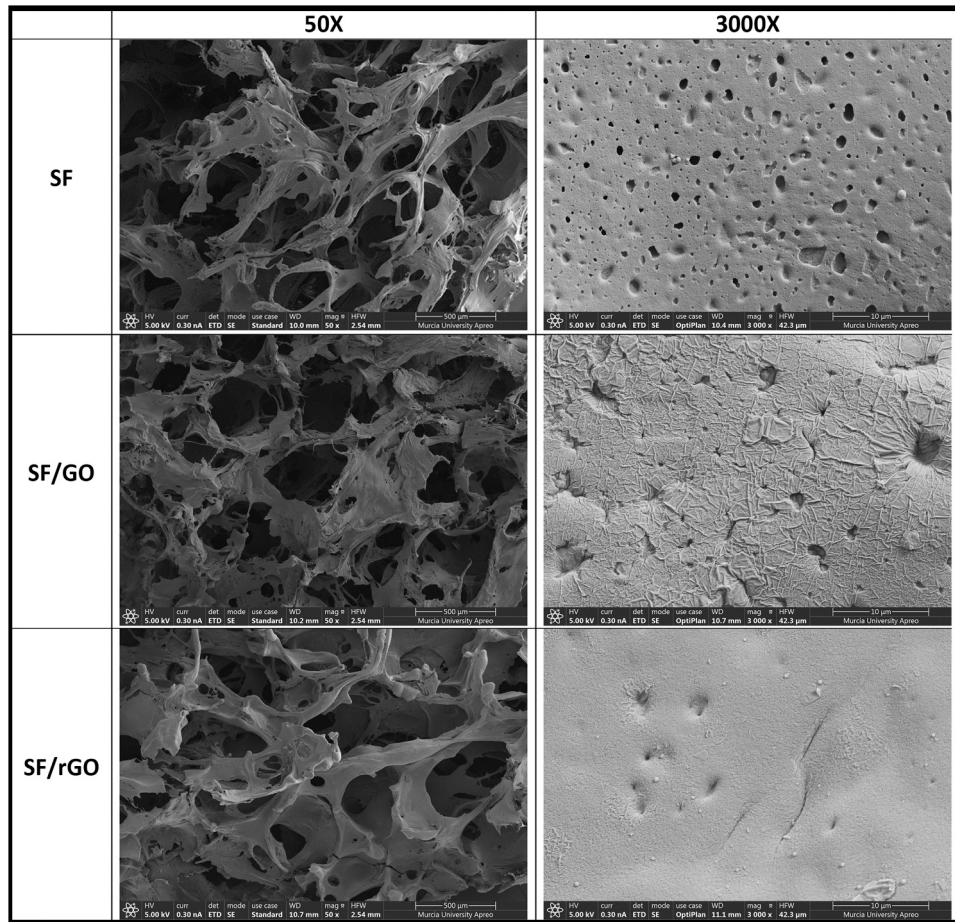|	Pore size – 50x (μm)	Pore size – 3000x (μm)	Water uptake (%)
SF	94,3 ± 21.0	* 0.6 ± 0.1	* 93.9 ± 0.2
SF/GO	120.5 ± 23.8	0.9 ± 0.1	91.6 ± 0.2
SF/rGO	128.9 ± 15.0	1.3 ± 0.2	92.1 ± 0.3

Fig. 1. Representative FESEM images for the assessment of scaffold microarchitecture. Magnifications: 50x (first column), 300x (second column).

Table 2

Mechanical properties of the different silk fibroin (SF) scaffolds produced evaluated until a 60% strain. "GO" or "rGO" refers to the presence of graphene oxide or reduced graphene. The data are expressed as average values ± standard deviation. **a** Indicates significantly different values (p < 0.05) SF vs SF/GO and **b** Indicates significantly different values (p < 0.05) SF vs SF/rGO.

Dry	Compressive force (N)	Compressive strength (kPa)	Compression modulus (kPa)
dSF	$34.1 \pm 3.2^{a,b}$	$1207.6 \pm 112.1^{a,b}$	$974.7 \pm 186.9^{a,b}$
dSF/GO	17.8 ± 2.3	510.4 ± 163.4	567.2 ± 131.1
dSF/rGO	20.0 ± 1.9	723.9 ± 51.0	473.5 ± 21.8
Wet	Compressive force (N)	Compressive strength (kPa)	Compression modulus (kPa)
wSF	1.6 ± 0.7	41.9 ± 17.4	34.1 ± 7.7
wSF/GO	1.9 ± 0.4	51.4 ± 7.5	40.8 ± 6.4
wSF/rGO	1.8 ± 0.4	46.2 ± 10.5	34.0 ± 4.9

AMELX, AMBN, and *DSPP* at 3, 7, 14 and 21 days using qPCR. As shown in Fig. 4, the early expression (at 3 days) of *ALP, Col1A1, ON, AMELX,* and *DSPP* was significantly higher in the SF/rGO scaffold than in the others, including with the OsteoDiff medium. While the overexpression of *DSPP* was maintained in the SF/rGOscaffold at all time points, the overexpression of *RUNX2, ON, ALP* and *Col1A1* in the SF scaffold was more pronounced at the late time points (14–21 days, Fig. 4 and Supplementary Fig. 3).

3.8. Mineralization assay

The mineralization potential was measured using a colorimetric assay based on Alizarin Red staining (Fig. 5). This assay showed that SF/GO and SF/rGO significantly increased the mineralization of hDPSCs when compared to the negative control (i.e., hDPSCs cultured in growth medium without any scaffold) and SF groups at 21 days(p < 0.05). Interestingly, more pronounced calcium deposition was observed in the positive control (OsteoDiff) at 7, 14 and 21 days (Fig. 5). Data of Abs405 and viable cell numbers obtained in each condition to obtain ratios are shown in Supplementary Table 1.

4. Discussion

In the present study, we investigated the effects of SF coated with GO or rGO and in a 3D conformation on the osteo/odontoblastic differentiation of hDPSCs. Several studies have proposed the use of biomaterial scaffolds in regenerative endodontics [27,28]. These materials should have certain characteristics to be able to be used for this purpose, such as providing a support to which the cells can adhere, allowing cell proliferation without affecting cell viability, and inducing their differentiation for the regeneration of the target tissue(s) [29]. The ability to allow adhesion and biocompatibility has already been described in silkworm fibroin and graphene oxide-coated silk fibroin in 2D structures [18,19]. Within this framework, this work aims to go one step further and evaluate the microarchitecture, mechanical and biological properties of three-dimensional SF coated with GO or rGO together with hDPSCs.

The microarchitecture and mechanical properties of scaffolds play a vital role in cell-to-cell communication and diffusion of nutrients,
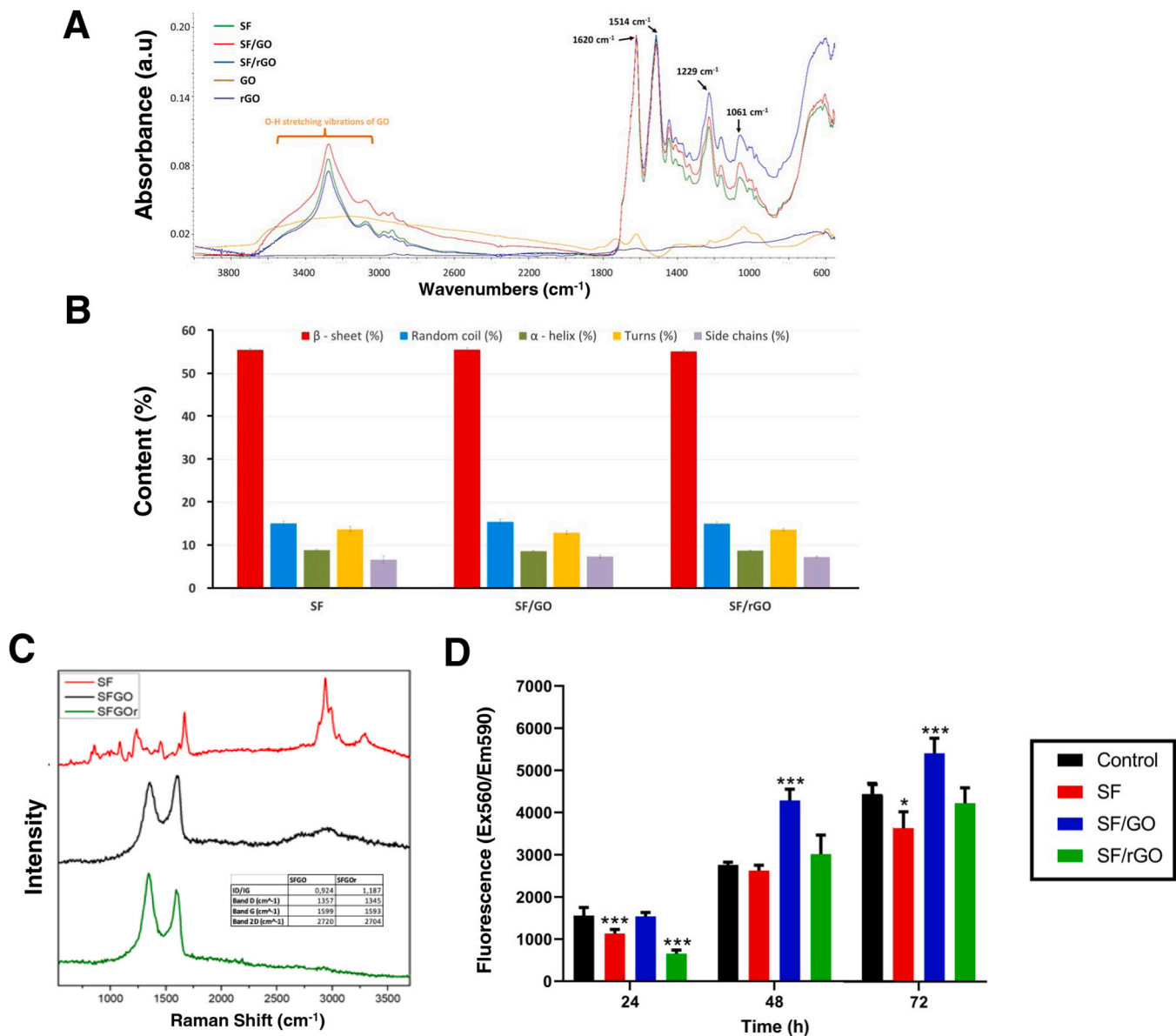
Fig. 2. A. Complete infrared spectra of the tested materials from the ATR-FTIR assay.**B.** Microstructural characterization of the tested materials. Data is presented as a % in content.**C.**Spectra of the tested materials from the Raman spectroscopy assay.**D.** Cytocompatibility assay results after 24, 48 and 72 hours of culture of hDPSCs with the tested materials. * **p < 0.001.

Table 3

Relative content of secondary structures of the scaffolds made by means of different treatments. The data are expressed as average values ± standard deviation.

	β-sheet (%)	Random coil (%)	α-helix (%)	β-turn (%)	Side chain (%)
SF	55.6 ± 0.4	15.1 ± 0.5	8.9 ± 0.1	13.8 ± 0.6	6.7 ± 0.9
SF/GO	55.6 ± 0.4	15.5 ± 0.6	8.6 ± 0.2	12.9 ± 0.4	7.4 ± 0.3
SF/rGO	55.2 ± 0.3	15.0 ± 0.5	8.8 ± 0.1	13.7 ± 0.3	7.3 ± 0.2

favouring a 3D microenvironment to promote odontoblastic differentiation [30]. SEM analysis revealed abundant pores with a size greater than 50 nm on the surface of the tested scaffolds, mainly between 50 nm and 600 μm. Pure silk fibroin (SF) scaffolds had a significantly smaller mean pore size than SF/GO and SF/rGO scaffolds. These results can be explained by the obstruction of the smaller pores of SF by the GO or rGO coverage, which is consistent with what is observed in the second column of Fig. 1. This is also in line with previous reports showing that scaffolds with a mean pore size of 65 μm presented superior results and could be a suitable alternative for pulp regeneration [31,32].

Regarding the water uptake values obtained in the present study (higher than 90%), it should be noted that they are within the range reported by other authors in porous scaffolds containing fibroin [33]. The average value of water uptake obtained in pure silk fibroin scaffolds was statistically higher than that of those containing GO or rGO (p < 0.05). This difference can be explained by a slight decrease in porosity associated with the surface adsorption of the graphene layer at different degrees of oxidation. The mechanical properties data obtained are also in the same range as those previously described by other authors in scaffolds containing fibroin [23,34]. The improvement in the mechanical properties may be related to the uniform dispersion of GO with high elastic modulus in the SF matrix and the intermolecular forces formed between the SF and GO. In addition, previous reports have been demonstrated that GO-coated or GO-incorporated scaffolds had the ability to induce the osteogenic differentiation of mesenchymal stem
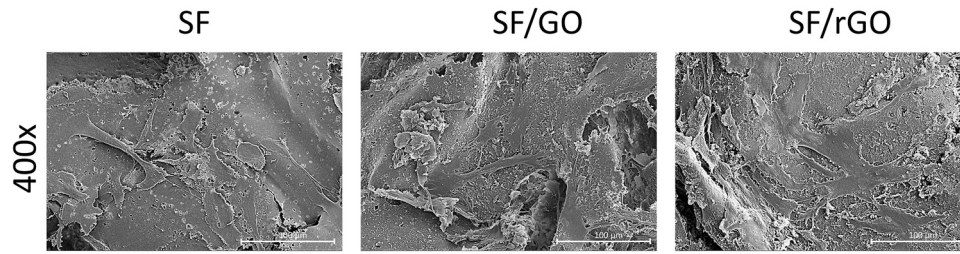
6

SF   SF/GO   SF/rGO

400x

Fig. 3. Representative SEM images for the assessment of hDPSCs superficial adherence and morphology. Magnification: 400x.

3 Days   7 Days   14 Days   21 Days
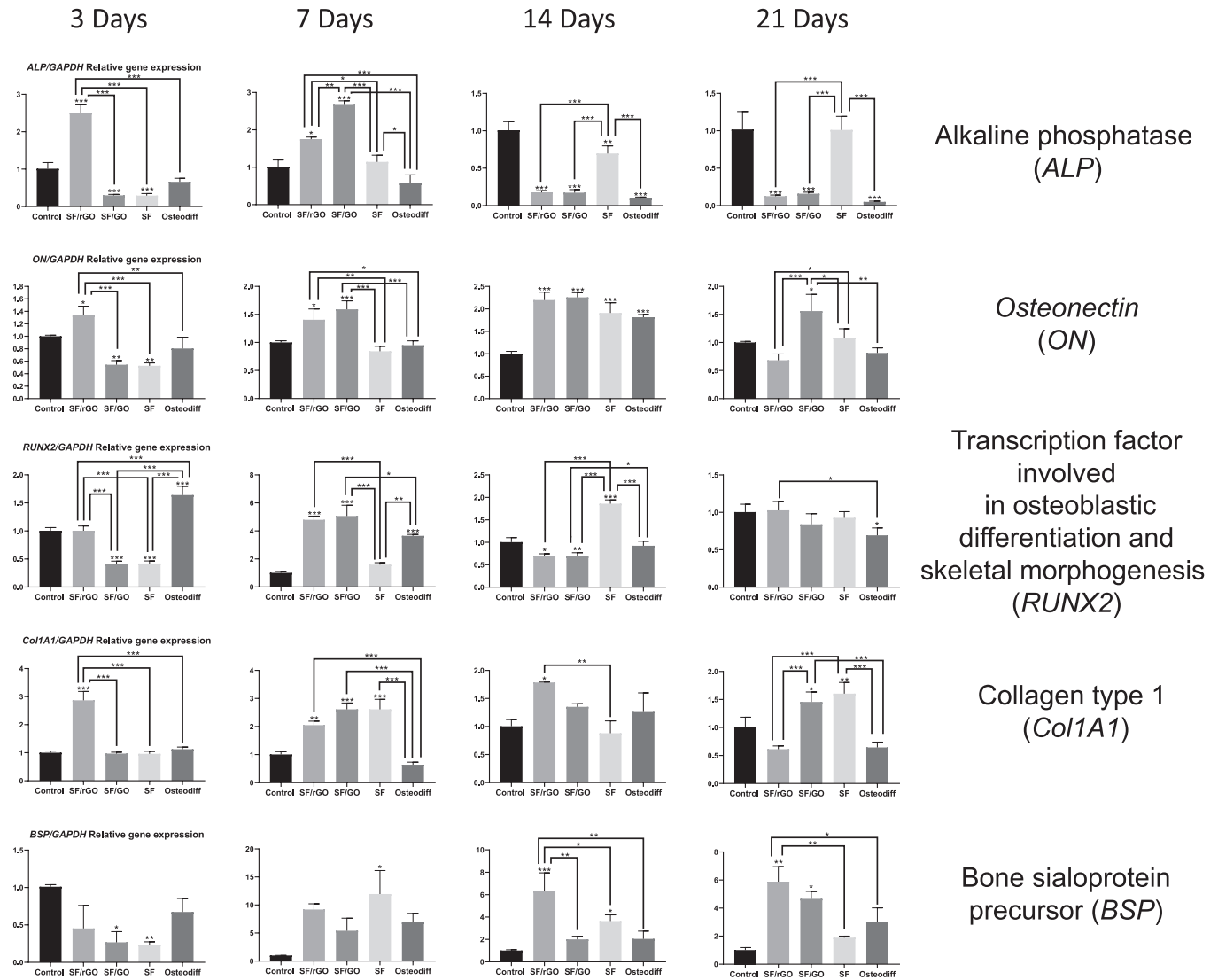

Alkaline phosphatase (*ALP*)

Osteonectin (*ON*)

Transcription factor involved in osteoblastic differentiation and skeletal morphogenesis (*RUNX2*)

Collagen type 1 (*Col1A1*)

Bone sialoprotein precursor (*BSP*)

Fig. 4. RT-qPCR osteogenic marker expression assay results after 3, 7,14 and 21 days of culture of hDPSCs with the tested materials. * p < 0.05; ** p < 0.01; *** p < 0.001.

cells due to the high elastic modulus and stiffness of the cell culture matrices [20]. ATR-FTIR evidenced that the secondary structures did not present differences between pure fibroin and fibroin coated with GO, showing a similar infrared spectrum in all tested scaffolds. Alternatively, Raman spectroscopy showed a greater number of defects in the links in SF/rGO scaffolds which could be attributed to a reduced amount of oxygenated groups or structural defects after the reduction process [35].

It has been suggested that GO and SF together in a proper configuration, alleviate the limitations imposed by individual biomaterials in terms of adhesion and proliferation, and have application potential for

clinical translational purposes [36]. In the present study, hDPSCs exhibited a fibroblastic spindle-like morphology with numerous extensions on the surface of the tested scaffolds under SEM. This cellular morphology may suggest that hDPSCs were able to attach to the surface of the scaffolds, as described in previous studies on the cytocompatibility of dental biomaterials [37,38]. Remarkably, no differences were observed between oxidized or reduced forms. Cell adhesion has previously been described with mouse fibroblasts cultured on graphene-coated substrates (glass, polydimethylsiloxane, or silicone) [39]. However, there is no information about SF/GO or SF/rGO scaffolds
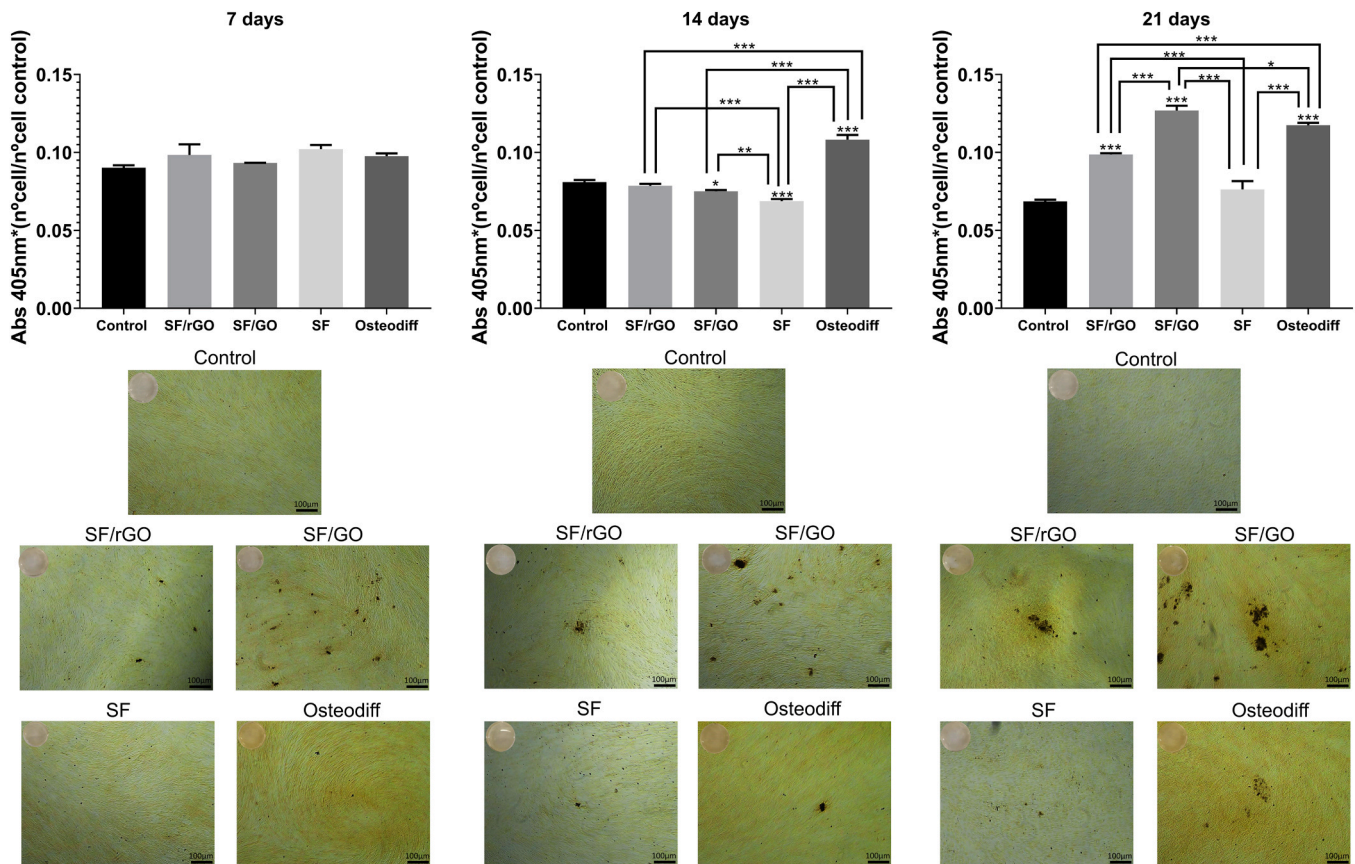
Fig. 5. Mineralization assay results after 7,14 and 21 days of culture of hDPSCs with the tested materials. * p < 0.05; *** p < 0.001.

using hDPSCs as the target cells.

The toxicity induced by graphene family nanomaterials (GFN) is concentration dependent, and, previous data have shown a high correlation between cell proliferation rates and GFN scaffold configurations [40,41]. Thus, the development of hybrid SF/GO or SF/rGO scaffolds could be considered as a support matrix to improve the mechanical properties of GFN and reduce the biotoxicity of GFN by adjusting their dosage. As shown in Fig. 2D, hDPSCs attached to the tested scaffolds were able to proliferate at a rate similar to that of the control without their metabolic activity being affected over time. Along the same lines, previous reports have demonstrated the cytocompatibility of fibroin and graphene in osteoblasts or periodontal ligament stem cells [42], but not in hDPSCs. In addition, the Annexin-V conjugated with phycoerythrin and 7-AAD was used to determine whether SF or GO could induce hDPSC apoptosis (Supplementary Fig 2.). Cells with positive Annexin V-FITC and negative PI staining and double positive Annexin V-FITC and PI staining were identified as apoptotic cells. It was observed that the proportion of apoptotic cells was not significant in the range of 2 mg/mL. Altogether, the aforementioned data indicate that graphene concentration in the tested scaffolds is biocompatible for hDPSCs.

Previous reports have highlighted the ability of graphene to induce the differentiation of periodontal ligament stem cells into osteoblasts and cementoblasts [43,44]. The tested scaffolds were able to induce overexpression of the *RUNX2*, *ALP*, and *COL1A1* genes in the first days of exposure, especially in the case of SF/rGO. These markers are involved in the early differentiation to osteoblasts/cementoblasts. For example, *RUNX2* is involved in triggering a series of molecular events involved in this process. Specifically, it is an activator of the expression of Osterix (*OSX*)[45]. The high expression of these genes in the absence of osteogenic inducers may be due to the spatial configuration of the scaffolds, especially with SF/rGO. It has been reported that mesenchymal stem cells (MSCs) cultured in three-dimensional environments showed high

attachment and cloning efficiency, rapid proliferation and longer lifespan [46]

In parallel, the *COL1A1* marker was overexpressed upon contact with all the scaffolds during the first 3 days of culture, while SF/rGO was the only scaffold to induce its late expression. *COL1A1* encodes the major component of collagen type 1: the collagen-enriched extracellular matrix (ECM), which plays a crucial role in osteoblast and cementoblast differentiation. In addition, type I collagen is the most abundant collagen found in bone and teeth [47]. Osteonectin (*ON*) is a calcium-binding glycoprotein with an affinity for collagen and is involved in the initiation of mineralization [48]. In our study, all scaffolds activate were found to activate the expression of this marker. The overexpression of these genes may be related to GO, which increases osteogenic differentiation of stem cells due to π–π stacking, electrostatic, and hydrophobic interactions with proteins [12]. Another structural gene of the extracellular matrix is bone sialoprotein (*BSP*), which appears to act as a mineralization nucleus for the deposition of the first apatite crystals during the process of mineralization [49]. Our findings showed an overexpression of *BSP* in SF/rGO and SF/GO-treated cells after 14 days of culture. In the case of *ALP*, an overexpression was observed in the first days of exposure only in the SF/rGO and SF/GO groups. *ALP* is a marker whose importance resides in the osteogenic differentiation process, since its enzymatic activity allows the removal of pyrophosphate, a natural inhibitor of tissue mineralization [50]. These results suggest that the scaffolds tested could play an important role in the regulation of ALP expression and activity [51,52].

Osteocalcin (*BGLAP*) is associated with the mineralization processes, and it is abundant in the extracellular matrix of bone, dentin, and cement tissues[53]. In our study, overexpression of osteocalcin was observed in SF/rGO and SF/GO scaffolds, whereas in the SF group its expression was discrete. Similarly, a significant upregulation of *DSPP* was observed in the SF/rGO and SF/GO groups. This marker, which is

generally produced by odontoblasts in the dental pulp and in small amounts in other similar tissues, is also involved in tissue mineralization [54,55]. Indeed, these results are consistent with previous studies reporting that the GO component of the mesoporous bioactive glass nanoparticles/GO composite plays an important role in the induction of mineralization in hDPSCs. Our results suggest that SF/rGO and SF/GO groups can effectively induce odontogenic differentiation.

Mineralization has been widely studied in the repair of tissues such as bone and dentin, and it is also an indication of odonto/osteoblastic differentiation [56]. In our study we evidenced that SF/GO and SF/rGO promoted calcium deposition. It has been described that these phenomena were enhanced with the use of chemical inducers for osteogenic differentiation [46,57]. However, other reports have been investigated that chemical and physical properties of graphene family nanomaterials promote differentiation without chemical inducers [58]. In agreement with Xie et al. [46] the tested hybrid scaffolds were cultured without the use of inducers and our data showed signs of mineralization. Interestingly, our results revealed more pronounced calcium deposits in SF/GO at day 21. All the data obtained suggest that a structure such as SF with GO or rGO promotes cell differentiation, both by increasing the expression of key osteo/odontogenic genes and by promoting the mineralization of the extracellular matrix.

The in vitro nature of the present study is its main limitation. The results of the present study were obtained under controlled laboratory conditions, where hDPSCs were cultured together with standardized samples of the scaffolds tested. Clinically, both the scaffolds and the cells may be exposed to different factors that may alter their response and behaviour, namely changes in pH, temperature, oxygen levels, different manipulation of the materials, host inflammatory response and underlying pathologies, among others, as shown for other dental biomaterials [59,60]. Therefore, the results should be interpreted as preliminary evidence, which is novel in terms of the use of a 3D model to perform the in vitro biological assays, but requires future evidence on animal models or clinical trials in order to confirm its results.

5. Conclusions

Our results suggested that SF/GO and SF/rGO scaffolds provided a suitable microenvironment for *h*DPSCs and promoted their proliferation with adequate microarchitectures and mechanical properties. Moreover, SF/GO and SF/rGO scaffolds promote hDPSC differentiation, both by increasing the expression of key osteo/odontogenic genes and by promoting the mineralization of the extracellular matrix.

Declaration of Competing Interest

The authors declare that they have no known competing financial interests or personal relationships that could have appeared to influence the work reported in this paper.

Appendix A. Supporting information

Supplementary data associated with this article can be found in the online version at doi:10.1016/j.dental.2023.12.009.

References

[1] Vallittu PK, Boccaccini AR, Hupa L, Watts DC. Bioactive dental materials-do they exist and what does bioactivity mean? Dent Mater 2018;34:693. -4.

[2] Sauro S, Babbar A, Gharibi B, Feitosa VP, Carvalho RM, Azevedo Rodrigues LK, et al. Cellular differentiation, bioactive and mechanical properties of experimental light-curing pulp protection materials. Dent Mater 2018;34:868. -78.

[3] Hadjichristou C, Papachristou E, Bonovolias I, Bakopoulou A. Three-dimensional tissue engineering-based Dentin/Pulp tissue analogue as advanced biocompatibility evaluation tool of dental restorative materials. Dent Mater 2020; 36:229. -48.

[4] Ahmed HMA, Nagendrababu V, Duncan HF, Peters OA, Dummer PMH. Developing a consensus-based glossary of controversial terms in Endodontology. Int Endod J 2023;56:788. -91.

[5] Tatullo M, Marrelli M, Paduano F. The regenerative medicine in oral and maxillofacial surgery: the most important innovations in the clinical application of mesenchymal stem cells. Int J Med Sci 2015;12:72. -7.

[6] Spagnuolo G, De Luca I, Iaculli F, Barbato E, Valletta A, Calarco A, et al. Regeneration of dentin-pulp complex: effect of calcium-based materials on hDPSCs differentiation and gene expression. Dent Mater 2023;39:485. -91.

[7] Kasoju N, Bora U. Silk fibroin in tissue engineering. Adv Health Mater 2012;1: 393–412.

[8] Kawakami M, Tomita N, Shimada Y, Yamamoto K, Tamada Y, Kachi N, et al. Chondrocyte distribution and cartilage regeneration in silk fibroin sponge. Biomed Mater Eng 2011;21:53–61.

[9] Kim KH, Jeong L, Park HN, Shin SY, Park WH, Lee SC, et al. Biological efficacy of silk fibroin nanofiber membranes for guided bone regeneration. J Biotechnol 2005; 120:327. -39.

[10] Li G, Kong Y, Zhao Y, Zhang L, Yang Y. Fabrication and characterization of polyacrylamide/silk fibroin hydrogels for peripheral nerve regeneration. J Biomater Sci Polym Ed 2015:1–34.

[11] Lozano-Pérez AA, Rodriguez-Nogales A, Ortiz-Cullera V, Algieri F, Garrido-Mesa J, Zorrilla P, et al. Silk fibroin nanoparticles constitute a vector for controlled release of resveratrol in an experimental model of inflammatory bowel disease in rats. Int J Nanomed 2014;9:4507. -20.

[12] Wu J, Zheng A, Liu Y, Jiao D, Zeng D, Wang X, et al. Enhanced bone regeneration of the silk fibroin electrospun scaffolds through the modification of the graphene oxide functionalized by BMP-2 peptide. Int J Nanomed 2019;14:733. -51.

[13] Eivazzadeh-Keihan R, Zare-Bakheir E, Aliabadi HAM, Gorab MG, Ghafuri H, Maleki A, et al. A novel, bioactive and antibacterial scaffold based on functionalized graphene oxide with lignin, silk fibroin and ZnO nanoparticles. Sci Rep 2022;12:8770.

[14] Xie H, Cao T, Franco-Obregon A, Rosa V. Graphene-induced osteogenic differentiation is mediated by the Integrin/FAK Axis. Int J Mol Sci 2019;20.

[15] Bressan E, Ferroni L, Gardin C, Sbricoli L, Gobbato L, Ludovichetti F, et al. Graphene based scaffolds effects on stem cells commitment. J Transl Med 2014;12: 296.

[16] Chen GY, Pang DW, Hwang SM, Tuan HY, Hu YC. A graphene-based platform for induced pluripotent stem cells culture and differentiation. Biomaterials 2012;33: 418. -27.

[17] Chung C, Kim YK, Shin D, Ryoo SR, Hong BH, Min DH. Biomedical applications of graphene and graphene oxide. Acc Chem Res 2013;46:2211. -24.

[18] Vera-Sánchez M, Aznar-Cervantes S, Jover E, García-Bernal D, Oñate-Sánchez RE, Hernández-Romero D, et al. Silk-fibroin and graphene oxide composites promote human periodontal ligament stem cell spontaneous differentiation into osteo/cementoblast-like cells. Stem Cells Dev 2016;25:1742. -54.

[19] Rodríguez-Lozano FJ, García-Bernal D, Aznar-Cervantes S, Ros-Roca MA, Algueró MC, Atucha NM, et al. Effects of composite films of silk fibroin and graphene oxide on the proliferation, cell viability and mesenchymal phenotype of periodontal ligament stem cells. J Mater Sci Mater Med 2014;25:2731. -41.

[20] Wang L, Lu C, Li Y, Wu F, Zhao B, Dong X. Green fabrication of porous silk fibroin/graphene oxide hybrid scaffolds for bone tissue engineering. RSC Adv 2015;5: 78660. -8.

[21] Pecci-Lloret MP, Vera-Sanchez M, Aznar-Cervantes S, Garcia-Bernal D, Sanchez RO, Pecci-Lloret MR, et al. Analysis of the adherence of dental pulp stem cells on two-dimensional and three-dimensional silk fibroin-based biomaterials. J Craniofacial Surg 2017;28:939. -43.

[22] Fernández-Merino MJ, Guardia L, Paredes JI, Villar-Rodil S, Solís-Fernández P, Martínez-Alonso A, et al. Vitamin C is an ideal substitute for hydrazine in the reduction of graphene oxide suspensions. J Phys Chem C 2010;114:6426. -32.

[23] Guan Y, You H, Cai J, Zhang Q, Yan S, You R. Physically crosslinked silk fibroin/hyaluronic acid scaffolds. Carbohydr Polym 2020;239.

[24] Madurga R, Ganán-Calvo AM, Plaza GR, Guinea GV, Elices M, Pérez-Rigueiro J. Production of high performance bioinspired silk fibers by straining flow spinning. Biomacromolecules 2017;18:1127. -33.

[25] Aznar-Cervantes SD, Pagán A, Candel MJ, Pérez-Rigueiro J, Cenis JL. Silkworm gut fibres from silk glands of samia cynthia ricini—potential use as a scaffold in tissue engineering. Int J Mol Sci 2022;23.

[26] Collado-Gonzalez M, Pecci-Lloret MR, Tomas-Catala CJ, Garcia-Bernal D, Onate-Sanchez RE, Llena C, et al. Thermo-setting glass ionomer cements promote variable biological responses of human dental pulp stem cells. Dent Mater 2018;34:932. -43.

[27] Dal-Fabbro R, Swanson WB, Capalbo LC, Sasaki H, Bottino MC. Next-generation biomaterials for dental pulp tissue immunomodulation. Dent Mater 2023;39:333. -49.

[28] Bakopoulou A, Georgopoulou A, Grivas I, Bekiari C, Prymak O, Loza K, et al. Dental pulp stem cells in chitosan/gelatin scaffolds for enhanced orofacial bone regeneration. Dent Mater 2019;35:310. -27.

[29] Singer L, Fouda A, Bourauel C. Biomimetic approaches and materials in restorative and regenerative dentistry: review article. BMC Oral Health 2023;23:105.

[30] Zhang W, Ahluwalia IP, Literman R, Kaplan DL, Yelick PC. Human dental pulp progenitor cell behavior on aqueous and hexafluoroisopropanol based silk scaffolds. J Biomed Mater Res A 2011;97:414. -22.

[31] Zhang Q, Yuan C, Liu L, Wen S, Wang X. Effect of 3-dimensional collagen fibrous scaffolds with different pore sizes on pulp regeneration. J Endod 2022;48:1493. -501.

[32] Sugiaman VK, Jeffrey, Naliani S, Pranata N, Djuanda R, Saputri RI. Polymeric scaffolds used in dental pulp regeneration by tissue engineering approach. Polym (Basel) 2023;15.

[33] Park HJ, Lee OJ, Lee MC, Moon BM, Ju HW, Lee JM, et al. Fabrication of 3D porous silk scaffolds by particulate (salt/sucrose) leaching for bone tissue reconstruction. Int J Biol Macromol 2015;78:215. -23.

[34] Yetiskin B, Okay O. High-strength silk fibroin scaffolds with anisotropic mechanical properties. Polymer 2017;112:61–70.

[35] Zhou M, Zhai Y, Dong S. Electrochemical sensing and biosensing platform based on chemically reduced graphene oxide. Anal Chem 2009;81:5603. -13.

[36] Norahan MH, Amroon M, Ghahremanzadeh R, Rabiee N, Baheiraei N. Reduced graphene oxide: osteogenic potential for bone tissue engineering. IET Nanobiotechnol 2019;13:720. -5.

[37] Lopez-Garcia S, Rodriguez-Lozano FJ, Sanz JL, Forner L, Pecci-Lloret MP, Lozano A, et al. Biological properties of Ceraputty as a retrograde filling material: an in vitro study on hPDLSCs. Clin Oral Invest 2023;27:4233. -43.

[38] Rodríguez-Lozano FJ, López-García S, García-Bernal D, Sanz JL, Lozano A, Pecci-Lloret MP, et al. Cytocompatibility and bioactive properties of the new dual-curing resin-modified calcium silicate-based material for vital pulp therapy. Clin Oral Investig 2021;25:5009. -24.

[39] Lin F, Du F, Huang J, Chau A, Zhou Y, Duan H, et al. Substrate effect modulates adhesion and proliferation of fibroblast on graphene layer. Colloids Surf B Biointerfaces 2016;146:785. -93.

[40] Malhotra R, Halbig CE, Sim YF, Lim CT, Leong DT, Neto AHC, et al. Cytotoxicity survey of commercial graphene materials from worldwide. npj 2D Mater Appl 2022;6.

[41] Wang J, Wu Y, Wang Y, Shuai Y, Xu Z, Wan Q, et al. Graphene oxide-coated patterned silk fibroin films promote cell adhesion and induce cardiomyogenic differentiation of human mesenchymal stem cells. Biomolecules 2023;13.

[42] Rodriguez-Lozano FJ, Garcia-Bernal D, Aznar-Cervantes S, Ros-Roca MA, Alguero MC, Atucha NM, et al. Effects of composite films of silk fibroin and graphene oxide on the proliferation, cell viability and mesenchymal phenotype of periodontal ligament stem cells. J Mater Sci-Mater Med 2014;25:2731. -41.

[43] Zhang X, Zhang H, Zhang Y, Huangfu H, Yang Y, Qin Q, et al. 3D printed reduced graphene oxide-GelMA hybrid hydrogel scaffolds for potential neuralized bone regeneration. J Mater Chem B 2023;11:1288. -301.

[44] Vera-Sanchez M, Aznar-Cervantes S, Jover E, Garcia-Bernal D, Onate-Sanchez RE, Hernandez-Romero D, et al. Silk-fibroin and graphene oxide composites promote human periodontal ligament stem cell spontaneous differentiation into osteo/cementoblast-like cells. Stem Cells Dev 2016;25:1742. -54.

[45] Liu Q, Li M, Wang S, Xiao Z, Xiong Y, Wang G. Recent advances of osterix transcription factor in osteoblast differentiation and bone formation. Front Cell Dev Biol 2020;8:601224.

[46] Han Xie TC, José Viana G, Antônio Hélio CN, Vinicius R. Two and three-dimensional graphene substrates to magnify osteogenic differentiation of periodontal ligament stem cells. Carbon 2015.

[47] Suzuki-Barrera K, Makishi S, Nakatomi M, Saito K, Ida-Yonemochi H, Ohshima H. Role of osteopontin in the process of pulpal healing following tooth replantation in mice. Regen Ther 2022;21:460. -8.

[48] Choi JY, Lee BH, Song KB, Park RW, Kim IS, Sohn KY, et al. Expression patterns of bone-related proteins during osteoblastic differentiation in MC3T3-E1 cells. J Cell Biochem 1996;61:609. -18.

[49] Vukovic M, Lazarevic M, Mitic D, Jaksic Karisik M, Ilic B, Andric M, et al. Acetylsalicylic-acid (ASA) regulation of osteo/odontogenic differentiation and proliferation of human dental pulp stem cells (DPSCs) in vitro. Arch Oral Biol 2022; 144:105564.

[50] Machla F, Sokolova V, Platania V, Prymak O, Kostka K, Kruse B, et al. Tissue engineering at the dentin-pulp interface using human treated dentin scaffolds conditioned with DMP1 or BMP2 plasmid DNA-carrying calcium phosphate nanoparticles. Acta Biomater 2023;159:156. -72.

[51] Zhang XF, Gurunathan S. Biofabrication of a novel biomolecule-assisted reduced graphene oxide: an excellent biocompatible nanomaterial. Int J Nanomed 2016;11: 6635. -49.

[52] Sun J, Li L, Xing F, Yang Y, Gong M, Liu G, et al. Graphene oxide-modified silk fibroin/nanohydroxyapatite scaffold loaded with urine-derived stem cells for immunomodulation and bone regeneration. Stem Cell Res Ther 2021;12:591.

[53] Lee AE, Choi JG, Shi SH, He P, Zhang QZ, Le AD. DPSC-derived extracellular vesicles promote rat jawbone regeneration. J Dent Res 2023;102:313. -21.

[54] Rosa V, Xie H, Dubey N, Madanagopal TT, Rajan SS, Morin JL, et al. Graphene oxide-based substrate: physical and surface characterization, cytocompatibility and differentiation potential of dental pulp stem cells. Dent Mater 2016;32:1019. -25.

[55] Xie H, Chua M, Islam I, Bentini R, Cao T, Viana-Gomes JC, et al. CVD-grown monolayer graphene induces osteogenic but not odontoblastic differentiation of dental pulp stem cells. Dent Mater 2017;33:e13–21.

[56] Wei XL, Luo L, Chen MZ, Zhou J, Lan BY, Ma XM, et al. Temporospatial expression of neuropeptide substance p in dental pulp stem cells during odontoblastic differentiation in vitro and reparative dentinogenesis in vivo. J Endod 2023;49: 276. -85.

[57] Lee WC, Lim CH, Shi H, Tang LA, Wang Y, Lim CT, et al. Origin of enhanced stem cell growth and differentiation on graphene and graphene oxide. ACS Nano 2011;5: 7334. -41.

[58] Luong-Van EK, Madanagopal TT, Rosa V. Mechanisms of graphene influence on cell differentiation. Mater Today Chem 2020;16.

[59] Domingos Pires M, Cordeiro J, Vasconcelos I, Alves M, Quaresma SA, Ginjeira A, et al. Effect of different manipulations on the physical, chemical and microstructural characteristics of Biodentine. Dent Mater 2021;37:e399–406.

[60] Chen B, Haapasalo M, Mobuchon C, Li X, Ma J, Shen Y. Cytotoxicity and the effect of temperature on physical properties and chemical composition of a new calcium silicate-based root canal sealer. J Endod 2020;46:531. -8.